AD-A095 295

SECURITY CLASSIFICATION OF THIS PAGE (When Data Entered)

(9) REPORT DOCUMENTATION PAGE

READ INSTRUCTIONS BEFORE COMPLETING FORM

1. REPORT NUMBER: NRL Memorandum Report 4390	2. GOVT ACCESSION NO.: AD-A095 295
3. RECIPIENT'S CATALOG NUMBER: (14) NRL-MR-4390	
4. TITLE (and Subtitle): A QUANTITATIVE SCHLIEREN SYSTEM FOR MEASURING RADIAL DENSITY PROFILES OF REDUCED DENSITY CHANNELS IN GASES	5. TYPE OF REPORT & PERIOD COVERED: Interim report on a continuing problem
	6. PERFORMING ORG. REPORT NUMBER
7. AUTHOR(s): M. Raleigh and J. R. Greig (16) RR011 09	8. CONTRACT OR GRANT NUMBER(s): (17)
9. PERFORMING ORGANIZATION NAME AND ADDRESS: Naval Research Laboratory, Washington, D.C. 20375	10. PROGRAM ELEMENT, PROJECT, TASK AREA & WORK UNIT NUMBERS: 61153N; RR011-09-41; 67-0871-0-0; and 61101E; 0; OR40AA
11. CONTROLLING OFFICE NAME AND ADDRESS: Office of Naval Research, Arlington, VA 22217 (11) 12 Defense Advanced Research Projects Agency Arlington, VA 22209 ATTN: Program Management/MIS	12. REPORT DATE: Feb [redacted] 81 (13) 26
	13. NUMBER OF PAGES: 25
14. MONITORING AGENCY NAME & ADDRESS (if different from Controlling Office): Naval Surface Weapons Center White Oak, MD 20910 ATTN: R-401 (15) NRDL-3718	15. SECURITY CLASS. (of this report): UNCLASSIFIED
	15a. DECLASSIFICATION/DOWNGRADING SCHEDULE

16. DISTRIBUTION STATEMENT (of this Report)

Approved for public release, distribution unlimited.

17. DISTRIBUTION STATEMENT (of the abstract entered in Block 20, if different from Report)

18. SUPPLEMENTARY NOTES

Research supported by the Office of Naval Research and by the Defense Advanced Research Projects Agency (DoD) ARPA Order No. 3718, monitored by the Naval Surface Weapons Center under Contract N60921-80-WR-W0189.

19. KEY WORDS (Continue on reverse side if necessary and identify by block number)

Quantitative
Schlieren
Radial density profile
Reduced density channel

20. ABSTRACT (Continue on reverse side if necessary and identify by block number)

A quantitative Schlieren system used to measure the radial density profiles of reduced density channels in gases is described. The system uses a simple, single path optical train and does not require a coherent light source. The cylindrical symmetry of the channels permits an Abel-like inversion of the path integrated bending of the light to yield the radial density profile. The inversion algorithm and a program using it are given and some experimental results are shown.

DD FORM 1473 EDITION OF 1 NOV 65 IS OBSOLETE
S/N 0102-014-6601

25 950

SECURITY CLASSIFICATION OF THIS PAGE (When Data Entered)

CONTENTS

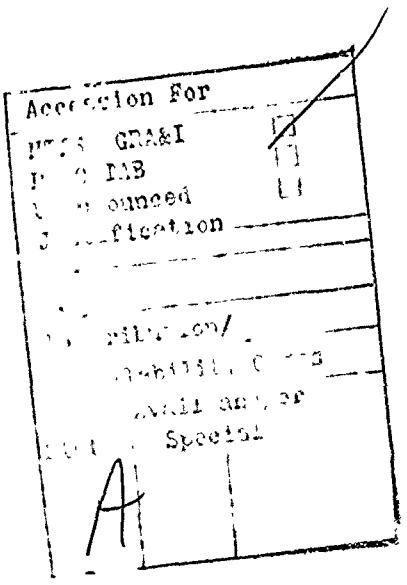

A QUANTITATIVE SCHLIEREN SYSTEM FOR MEASURING RADIAL DENSITY PROFILES OF REDUCED DENSITY CHANNELS IN GASES

I. INTRODUCTION

Hot, reduced-density channels through gaseous atmospheres are of interest for a variety of reasons. In future inertial confinement fusion reactors such channels will probably be used to transport the charged particle beams through the reactor atmosphere to the pellet.[1,2] While in the atmosphere every flash of lightning creates a hot, reduced-density channel and it is in the details of the process of channel cooling that atmospheric nitrogen is fixed.[3] In experiments at NRL[4,5] pertinent to both these areas, the channels produced in the atmosphere by laser-guided and unguided electric discharges have been studied using a quantitative Schlieren technique.[6]

This technique detects the total angular deflection of light passing through the channel as a function of the lateral distance from the channel axis. An Abel-like inversion is applied to find the radial density gradient as a function of radius within the channel. The density gradient is then integrated to yield the density profile. The ability of this system to detect angular deflections is dependant on a geometric ray approximation being valid throughout the optical train. This implies a limit on the narrowness of the slit used in the system which in turn implies a minimum readable angular deflection of $\sim 10^{-4}$ radians. This sensitivity is adequate to measure the strong density gradients encountered in the channels. On the other hand, the total deflections encountered are sufficiently small that the light rays may be approximated as passing straight across the channel when the incremental deflections along the path are summed.

Manuscript submitted October 24, 1980.

II. A DESCRIPTION OF THE SYSTEM

The quantitative Schlieren system is shown in Fig. 1. The ruby laser produces a parallel beam of light ~ 1 cm in diameter. The laser energy is ~ 2J and the pulse width is ~ 25 ns FWHM. The first cylindrical lens (a) brings the beam to a horizontal line focus (b). The light then re-expands vertically until it impinges on the first large lens (c) as a slender vertical elipse. This lens is positioned at its focal distance from the line focus (b) and stops the vertical expansion of the light. At the same time it causes the light to focus sideways to produce a vertical line focus (d). The light re-expands horizontally beyond the vertical line focus until falling as another slender vertical elipse on the symmetrically placed second large lens (e). This lens restores the horizontal parallelism of the light and focuses it vertically to produce a second horizontal line focus at the inclined slit (*f*). The slit has a width of ~.5 mm and light rays preserve their identity in transiting the slit. The central portion of the horizontal line focus emerges from the slit, expanding vertically, and passes through the center of the second cylindrical lens (g). This lens does not affect the vertical expansion but projects an enlarged version of the horizontal extent of the emergent light on to the film (h). This results in a vertical band of light on the film (Fig. 2).

When a disturbance is present (*i*), the light at various offsets may be bent vertically: such rays are indicated by dotted lines in Fig. 1. These rays, because of their angular deviation, reach a horizontal line focus at the inclined slit (*f*) which is above that formed by the undeviated rays. Therefore, a non-central portion of this light emerges from the slit and is projected sideways by the second cylindrical lens. The vertical path of these rays is nearly the same beyond the slit as if they were not deflected so they fall in their appropriate position vertically on the film. The image on the film becomes therefore a plot of angular deflection versus offset. For a cylindrically symmetric channel there will result a record which is antisymmetric about the channel center (Fig. 2).

The magnification of the offset distance depends on the ratio of the focal length (f_2) of the second large lens (*e*) and the distance (d_1) from the inclined slit (*f*) to the film (*h*).

$$\frac{y_{\text{film}}}{y_{\text{channel}}} = \frac{d_1}{f_2}. \tag{1}$$

The angular magnification is determined by the focal length (f_2) of the second large lens (e), the angle of inclination (ϕ) of the slit (f), the focal length (f_3) of the second cylindrical lens (g), and the distance (d_2) from the second cylindrical lens (g) to the film (h).

$$\frac{x_{film}}{\theta} = \frac{f_2(d_2-f_3)}{f_3 \tan\phi} \left[\frac{cm}{rad.}\right]. \tag{2}$$

The offset magnification may be experimentally calibrated by inserting an opaque object of known size. The angular magnification may be experimentally calibrated by inserting either a glass wedge of known deviation or an extremely long focal length lens.

III. DATA ANALYSIS

The rate of deflection of a light ray traveling in the z direction due to a transverse gradient in the refractive index ($\partial\eta/\partial y$) is given by[7]

$$\frac{d\theta}{dz} = \frac{1}{\eta}\frac{\partial\eta}{\partial y}. \tag{3}$$

In the channels being studied at NRL the refractive index is determined by the density of polarizable neutral molecules and atoms and is near unity. In that case it may be shown that the Clausius-Mossotti relationship between the refractive index (η) and the species polarizability (α) reduces to[8]

$$\eta - 1 \approx 2\pi n\alpha \tag{4}$$

where n is the species number density. We may therefore relate the rate of deflection to the transverse gradient in number density.

$$\frac{d\theta}{dz} = \frac{1}{\eta}\frac{\partial\eta}{\partial y} \approx \frac{\partial\eta}{\partial y} \approx 2\pi\alpha\frac{\partial n}{\partial y} \tag{5}$$

Values of $2\pi\alpha$ are given in Table 1 for several gases.[9,10,11,12] The polarizabilities of a molecule and an atom for normally diatomic gases obey

$$2\alpha(M) \geq \alpha(M_2) \geq \alpha(M).$$

For the situations considered here, the fractional dissociation (δ) is $\leqslant 0.2$ and for simplicity we have taken

$$\alpha(M) = \alpha(M_2),$$

which results in an underestimate of the density on the channel axis by $\sim 10\%$.

We will assume the reduced density channels are cylindrically symmetric and that the light traverses them along straight chords. We will also assume the channel consists of concentric shells, each characterized by a constant radial density gradient (Fig. 3). In this diagram each shell is identified by its inner radius so that $(\partial n/\partial r)_i$ represents the constant radial density gradient characterizing the shell with inner radius r_i. The outside of the channel has radius r_N and the innermost cylinder is assumed to be uniform giving $N-1$ nontrivial shells. A ray is identified by the radius of the interior shell to which it is tangent (r_j). The radius is equal to the offset of the ray.

The incremental deflection along a chord within one shell may be evaluated analytically (Fig. 4). Because the channel is cylindrically symmetric, the total bending of the light ray when passing both into and out of a shell may be found by integrating $\partial\theta/\partial z$ along the inbound chord segment and doubling the result. It is convenient to use r as the variable of integration. The variables l and r are related via

$$l = (r^2 - r_j^2)^{1/2} - (r_i^2 - r_j^2)^{1/2} \tag{6}$$

and

$$dl = (r^2 - r_j^2)^{-1/2}\, r\, dr. \tag{7}$$

The transverse density gradient is related to the radial gradient via

$$\frac{\partial n}{\partial y} = \sin\psi\, \frac{\partial n}{\partial r} = \frac{r_j}{r}\, \frac{\partial n}{\partial r}. \tag{8}$$

The path integral for the total bending in one shell is therefore given by

$$\Delta\theta = 2\int \frac{\partial \eta}{\partial y}\, dl = 2\int_{r_j}^{r_{i-1}} \left(\frac{2\pi\alpha\, r_j}{r}\, \frac{\partial n}{\partial r}\right)\left(\frac{r\, dr}{\sqrt{r^2 - r_j^2}}\right)$$

$$= 4\pi\alpha\, r_j \left(\frac{\partial n}{\partial r}\right)_i \int_{r_i}^{r_{i-1}} \frac{dr}{\sqrt{r^2 - r_j^2}}$$

$$= 4\pi\alpha\, r_j \left(\frac{\partial n}{\partial r}\right)_i \ln\left\{\frac{r_{i+1} + \sqrt{r_{i+1}^2 - r_j^2}}{r_i + \sqrt{r_i^2 - r_j^2}}\right\}. \tag{9}$$

We may evaluate the total deflection of the ray tangent to r_j (see Fig. 3) by summing the bending in each shell traversed by the ray

$$\theta_j = 4\pi\alpha\, r_j \sum_{i=j}^{N} \left(\frac{\partial n}{\partial r}\right)_i \ln\left\{\frac{r_{i+1} + \sqrt{r_{i+1}^2 - r_j^2}}{r_i + \sqrt{r_i^2 - r_j^2}}\right\}. \tag{10}$$

We may find an inversion of this equation by dividing by r_j and separating the term representing the innermost contribution to the bending

$$\frac{\theta_j}{r_j} = 4\pi\alpha \left(\frac{\partial n}{\partial r}\right)_j \ln\left\{\frac{r_{j+1} + \sqrt{r_{j+1}^2 - r_j^2}}{r_j}\right\} + 4\pi\alpha \sum_{i=j+1}^{N} \left(\frac{\partial n}{\partial r}\right)_i \ln\left\{\frac{r_{i+1} + \sqrt{r_{i+1}^2 - r_j^2}}{r_i + \sqrt{r_i^2 - r_j^2}}\right\} \tag{11}$$

We may now solve for $(\partial n/\partial r)_j$

$$\left(\frac{\partial n}{\partial r}\right)_j = \frac{\theta_j}{4\pi\alpha\, r_j \ln\left\{\frac{r_{j+1} + \sqrt{r_{j+1}^2 - r_j^2}}{r_j}\right\}} - \frac{\sum_{i=j+1}^{N} \left(\frac{\partial n}{\partial r}\right)_i \ln\left\{\frac{r_{i+1} + \sqrt{r_{i+1}^2 - r_j^2}}{r_i + \sqrt{r_i^2 - r_j^2}}\right\}}{\ln\left\{\frac{r_{j+1} + \sqrt{r_{j+1}^2 - r_j^2}}{r_j}\right\}}. \tag{12}$$

This equation allows us to find $(\partial n/\partial r)_j$ given θ_j provided we already know $(\partial n/\partial r)_i$ for all $i > j$. We may therefore find all values of $(\partial n/\partial r)$ by successive solutions of this equation starting with $j = N-1$ and working inwards. This inversion forms the basis of the computer program used to analyze the data. Having found $\partial n/\partial r$ as a function of radius, integration yields the density as a function of radius.

$$n(r) = n(\infty) - \int_r^{\infty} \frac{\partial n}{\partial r}\, dr. \tag{13}$$

The computer program carries this integration inwards one shell at a time using the assumption that $(\partial n/\partial r)$ is constant within each shell.

$$n_j = n_{j-1} - \left(\frac{\partial n}{\partial r}\right)_j (r_{j-1} - r_j) \tag{14}$$

A listing of the computer program is given in the Appendix.

By applying equation (9) to the piecewise analytic density profile shown in Fig. 5, a set of test data was generated to check the inversion program. The fit achieved by the program when run on the test data is indicated on the figure.

A refinement which has been added to the inversion program is a correction for the small lateral position error that results when the light is deflected. This aberration is seen in Fig. 2 where the deflected line overhangs the undisturbed portions. The size of this aberration is proportional to the angular deflection and the raw data is thus readily corrected prior to inversion. The correction to the lateral position is found as follows

$$y_{\text{real}} = y_{\text{measured}} + \theta(y)\, f_2 \tag{15}$$

where bending away from the channel represents a positive angle and is the type of deflection given by a reduced density cylinder.

A test which has been made on the density profiles from the ohmicly heated channels is to count the total number of equivalent molecules in a cylindrical volume which contains the disturbed region and to compare this to the number of molecules in an equal size cylinder of ambient air. Account must be taken of the dissociation in the hot inner parts of the channel. The fractional dissociation (δ) is defined by the relation

$$(1 + \delta) = \frac{n}{m} \tag{16}$$

where n is the particle density and m is the molecular density. A plot of $(1 + \delta)$ versus T for air in equilibrium at elevated temperatures is shown in Fig. 6. An approximation to this data is shown by the dotted line and is given by

$$(1 + \delta) \simeq \begin{cases} 9.362 \times 10^{-5}\, T + .751 & T > 2650°K \\ 1 & T \leqslant 2650°K \end{cases} \quad \text{or} \tag{17}$$

We are interested in density profiles at times when pressure equilibrium is established across the channel. Therefore within the channel we may write

$$nkT = 1\ \text{atm.} \tag{18}$$

Equations 16, 17, and 18 represent three equations for the unknowns m, $(1 + \delta)$, and T. We may eliminate $(1 + \delta)$ and T resulting in the following solution for m.

$$m = \left\{ \begin{array}{c} \text{the lesser of} \\ \dfrac{n^2}{6.875 \times 10^{17} + .751\, n} \\ \text{or} \\ n \end{array} \right\}. \tag{19}$$

Using this equation we convert the particle density (n) as a function of radius, into an equivalent molecule density (m). In the over pressured region behind the shock wave application of Equation 19 assigns zero dissociation. We then count up the equivalent molecules per unit length

$$M = \int_0^{r_N} m(r)\, 2\pi\, r\, dr. \tag{20}$$

The program carries this integration inwards one shell at a time assuming $m(r)$ varies linearly within each shell.

$$M_j = M_{j+1} + \frac{2\pi}{3} g (r_{j+1}^3 - r_j^3) + \pi h (r_{j+1}^2 + r_j^2) \tag{21}$$

where g is the slope of the linear variation in $m(r)$ and h is the intercept.

$$g = \frac{m_{j+1} - m_j}{r_{j+1} - r_j} \tag{22}$$

$$h = m_j - g r_j. \tag{23}$$

The program also computes the comparison value of $\pi r_0^2 m_0$ where m_0 is the ambient value.

IV. SOME EXPERIMENTAL RESULTS

Figure 7 shows the density profile that results when the data given in Fig. 2 is inverted. The figure also shows the result of a hydrocode simulation[13] for two possible initial conditions. The actual channel is not perfectly symmetric as may be seen from the irregular outline in the Schlieren photograph in Fig. 2. The channel also becomes turbulent with time which indicates the presence of vorticity within the channel. This lack of symmetry results in errors which accumulate as the inversion proceeds inward. The system cannot therefore resolve the low (1/20 atmospheric) interior density predicted by theory. However shape is predicted correctly down to densities of ~ 1/10 atmosphere and the overall agreement between calculated and measured density profiles is well within the uncertainty in the input data (energy deposited, deposition profile, and time) fed to the computer simulation.

V. CONCLUSIONS

The quantitative Schlieren technique described in this paper is best adapted to measuring the density profiles of highly symmetric (cylindrical or spherical) disturbances in gases. It is a low sensitivity system useful for viewing disturbances with strong density gradients. The ability to resolve low absolute interior densities is dependent upon the degree of symmetry and lack of interior structure (e.g., shock waves or turbulence) of the disturbance. Disturbances likely to meet these requirements include electric sparks, laser breakdowns, and channels formed by intense, relativistic particle beams, particularly those possessing a smooth (i.e., Bennett) profile.

The technique directly compliments normal Schlieren photography. It identifies the sign and magnitude of the angular light deflections leading to darkened regions in a normal Schlieren photograph. This may be used to identify areas of compression and rarefaction without actually inverting the data.

VI. ACKNOWLEDGMENTS

We wish to acknowledge discussions with Drs. H. L. Crannell and C. W. Werntz of the Catholic University of America regarding the optical behavior of the system and the assistance of Drs. J. C. Halle, and R. B. Fiorito in developing the inversion program.

VII. APPENDIX: A Basic Computer Program for Inverting Schlieren Data

In this program:

AS is simply a name for data identification

$M1$ is the offset magnification as defined by Eq. (1).

$M2$ is the angular magnification as defined in Eq. (2).

$N1$ is the number of pairs of data points, $R(J)$ and $O(J)$, where $R(J)$, is the offset on the record, y_{film}, and $O(J)$ is the deflection, χ_{film}. These are shown in figure 5b.

Test data is included with the program for the analytic model in figure 5, we note that for this model the value of $\pi r_N^2 m_o$ is meaningless and should not be compared with the numbers of equivalent molecules within the raduis r_N.

```
 80/10/01. 11.44.52.
PROGRAM   JRGMR

00100 REM CYLINDRICAL LENS SCHLIEREN INVERSION
00110 REM INPUT A$,M1,M2
00120 REM A$=RECORD NAME,M1=RADIUS MAG,M2=ANGLE MAG (CM/RADIAN)
00130 REM DATA INPUT N1,R(J),O(J)
00140 REM N1=NO PTS,R(J)=RAD (CM),O(J)=ANGLE (
00150 REM DATA INPUT WITH INCREASING RADIUS
00160 DIM R(100),O(100),X(100),D(100),N(100),P(100)
00170 READ A$,M1,M2,N1
00180 PRINT "FOR RECORD" A$
00190 FOR I=1 TO N1
00200 READ R(I), O(I)
00210 O(I)=O(I)/M2
00220 R(I)=(R(I)/M1)+76.2*O(I)
00230 REM ABBERATION CORRECTION INCLUDED
00240 NEXT I
00250 R(0)=0
00260 R(N1+1)=R(N1)*2
00270 N(N1)=2.55E19
00280 P(N1)=0
00290 M=0
00300 R1=R(N1)
00310 R2=R(N1+1)
00320 X(N1)=O(N1)/(2*R1*LOG((R2+SQR(R2^2-R1^2))/R1))
00330 FOR J=N1-1 TO 2 STEP -1
00340 R1=R(J)
00350 R4=R(J+1)
00360 Y=0
00370 C=LOG((R4+SQR(R4^2-R1^2))/R1)
00380 FOR I=N1 TO J+1 STEP -1
00390 R3=R(I+1)
00400 R2=R(I)
00410 Y=Y+X(I)*LOG((R3+SQR(R3^2-R1^2))/(R2+SQR(R2^2-R1^2)))
00420 NEXT I
00430 X(J)=O(J)/(2*R1*C)-Y/C
00440 D(J)=X(J)/10.84E-24
00450 REM INTEGRATE DENSITY DERIVITIVE
00460 N(J)=N(J+1)-D(J)*(R2-R1)
00470 REM EQU. MOL. COUNT
00480 P(J)=N(J)^2/(.751*N(J)+6.875E17)
00490 IF P(J)<N(J) THEN 00510
00500 P(J)=N(J)
00510 G=(P(J+1)-P(J))/(R2-R1)
```

```
00520 H=P(J)-G*R1
00530 M=M+2.094*(R2^3-R1^3)*G+3.1416*(R2^2-R1^2)*H
00540 NEXT J
00550 N(1)=N(2)
00560 N(1)=N(2)
00570 M=M+3.1416*P(2)*R1^2
00580 REM COMPARISON VALUE
00590 Q=2.55E19*3.1416*R(N1)^2
00600 PRINT USING 00610
00610 :RADIUS          DENSITY
00620 :#.##^^^^^       #.##^^^^^
00630 :CM              CM-3
00640 FOR J=1 TO N1
00650 PRINT USING 00620 ,R(J),N(J)
00660 NEXT J
00670 PRINT USING 00630
00680 PRINT USING 00700
00690 PRINT USING 00710 ,M,Q
00700 :EQU. MOLS.      COMPARE
00710 :#.##^^^^^        #.##^^^^^
00720 REM DATA IMPUT
00730 DATA " ANALYTIC ",2.5,2800,21
00740 DATA 0,0,.243,.103,.486,.208,.728,.317
00750 DATA .971,.432,1.212,.555,1.453,.692,1.692,.849
00760 DATA 1.929,1.040,2.162,1.298,2.367,1.959,2.616,1.971
00770 DATA 2.867,1.961,3.119,1.926,3.373,1.865,3.629,1.774
00780 DATA 3.888,1.649,4.149,1.480,4.415,1.250,4.688,.912
00790 DATA 5.000,0
00800 END
READY.
RUN

 80/10/01. 11.46.22.
PROGRAM   JRGMR

FOR RECORD ANALYTIC
RADIUS          DENSITY
 .00E+000       1.01E+018
1.00E-001       1.01E+018
2.00E-001       1.00E+018
3.00E-001       9.99E+017
4.00E-001       9.99E+017
5.00E-001       9.99E+017
6.00E-001       9.99E+017
7.00E-001       9.99E+017
8.00E-001       9.99E+017
9.00E-001       1.00E+018
1.00E+000       1.00E+018
1.10E+000       3.45E+018
1.20E+000       5.90E+018
1.30E+000       8.35E+018
1.40E+000       1.08E+019
```

```
1.50E+000       1.33E+019
1.60E+000       1.57E+019
1.70E+000       1.82E+019
1.80E+000       2.06E+019
1.90E+000       2.31E+019
2.00E+000       2.55E+019
CM              CM-3
EQU. MOLS.       COMPARE
1.24E+020         3.20E+020

SBU       0.732 UNTS.

RUN COMPLETE.
```

VIII. REFERENCES

1. G. Yonas, Sci. Amer. *239* (5), 50-61 (1978)

2. P.A. Miller, R.F. Butler, M. Cowan, J.R. Freeman, J.W. Poukey, T.P. Wright, and G. Yonas, Phys. Rev. Lett. *39*, 92-94 (1977).

3. R.D. Hill, R.G. Rinker, and H.D. Wilson, J. Atmos. Sci. *37*, 179-192 (1980).

4. M. Raleigh, J.R. Greig, R.E. Pechacek, and E. Laikin, NRL MR 4380 (1980) [see also M. Raleigh, J.R. Greig, and R.E. Pechacek, Bull. Am. Phys. Soc. 24, 978 (1979) and M. Raleigh, J.C. Halle, R.E. Pechacek, R.B. Fiorito, E. Laikin, and J.R. Greig, IEEE Conference Recorded — Abstracts, 1980 IEEE International Conference on Plasma Science, p. 83 (May 1980)].

5. M. Raleigh, J.D. Sethian, L. Allen, J.R. Greig, R.B. Fiorito, and R.F. Fernsler, NRL MR 4220 (1980) [see also J.R. Greig, M. Raleigh, R.B. Fiorito, J.D. Sethian, R.F. Fernsler, and L. Allen, IEEE Conference Record — Abstracts, 1980 IEEE International Conference on Plasma Science, p. 82, (May 1980)].

6. L.A. Vasil'ev, "Schlieren Methods," Israel Program for Scientific Translations, New York (1971), p. 23

7. R.H. Lovberg in "Plasma Diagnostic Techniques," Edited by R.H. Huddlestone and S.L. Leonard, Academic Press, New York (1965), Chapt. 3, p. 46

8. R.A. Alpher and D.R. White in "Plasma Diagnostic Techniques," Edited by R.H. Huddlestone and S.L. Leonard, Academic Press, New York (1965) Chapt. 10, p. 440

9. C.W. Allen, "Astrophysical Quantities," The Athlone Press, London (1973), p. 92

10. H.R. Griem, "Plasma Spectroscopy," McGraw-Hill Book Company, New York (1964), p. 42

11. W.L. Wiese, M.W. Smith, and B.M. Glennon, "Atomic Transition Probabilities," National Bureau of Standards, (1966), NSRDS-NBS4 Vol. I.

12. R.A. Alpher and D.R. White, Phys. Fluids 2, 153 (1959)

13. S. Kainer and M. Lampe, NRL MR 4247 (1980)

Table 1 — Polarizabilities of Various Species

Species	$2\pi\alpha$ (cm^3)	Ref.
H_2	5.14×10^{-24}	9
H	$6.62 \times 10^{-24*}$	10,11
N_2	1.104×10^{-23}	9
N	7.1×10^{-24}	12
O_2	1.06×10^{-23}	9
O	4.8×10^{-24}	12
Air	10.84×10^{-24}	9

*estimated based on oscillator frequencies & strengths

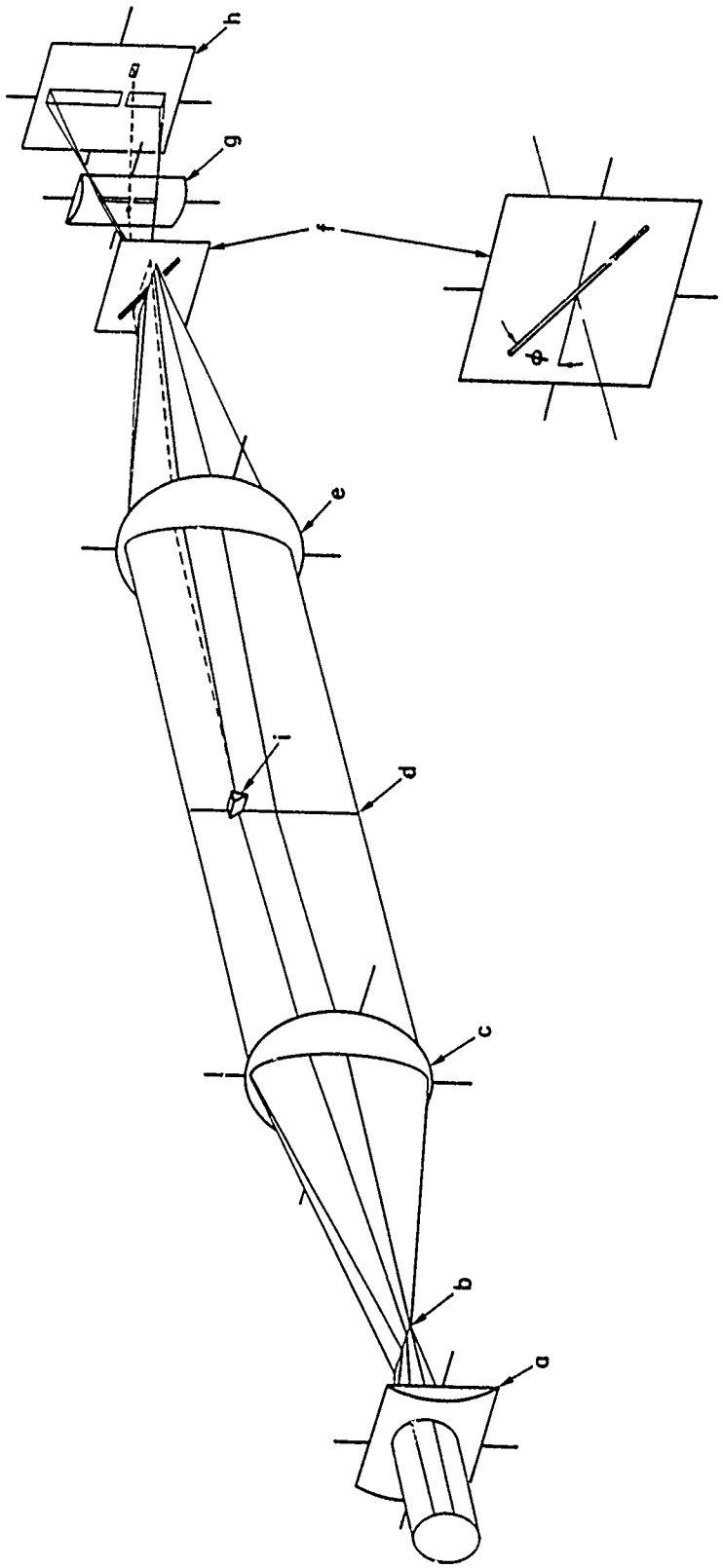

Fig. 1 — The optical train of the quantitative Schlieren system.

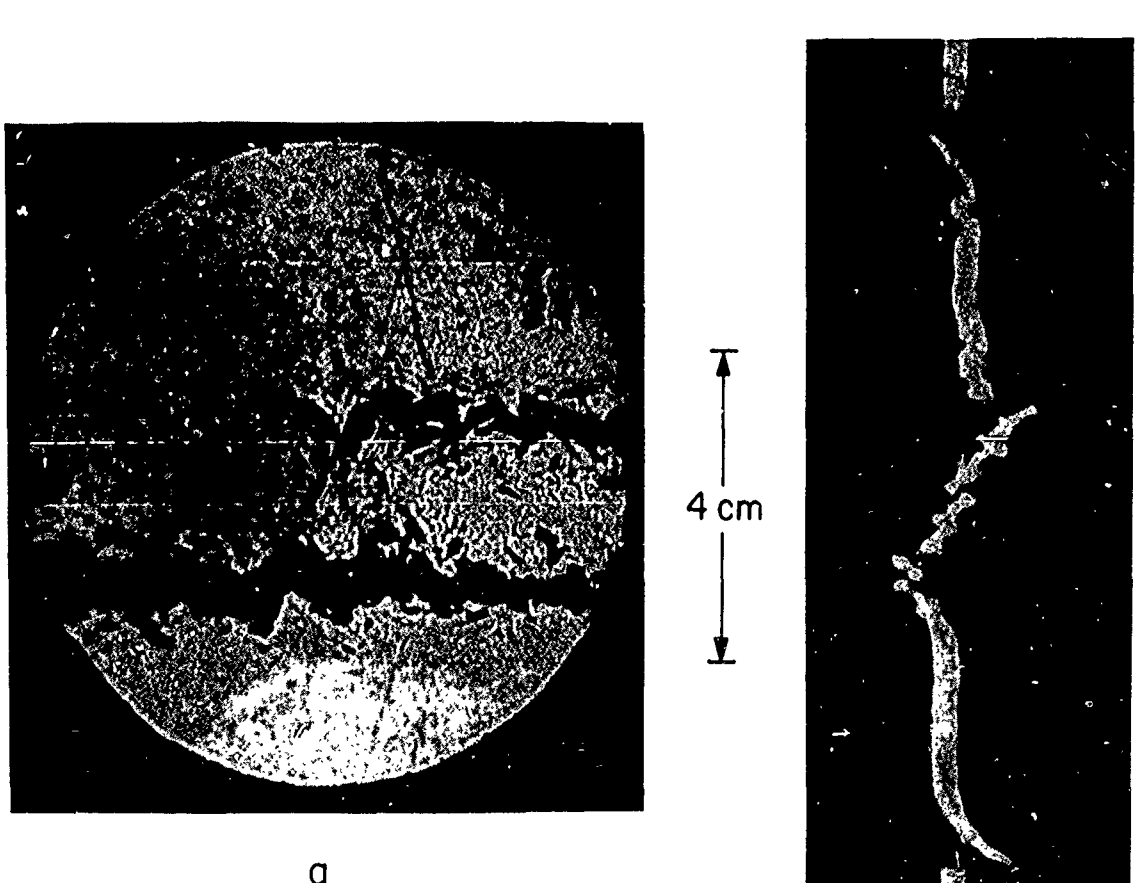

Fig 2 – Data for a laser initiated ohmicly heated reduced density channel. a) A Schlieren photograph taken with a pinhole in place of the usual knife edge b) The quantitative Schlieren photograph showing deflections due to both the reduced density channel and the outward going shock wave Both photographs were taken ~ 85μs after the high voltage discharge which causes the ohmic heating. Exposure time for both photographs was ~25 ns.

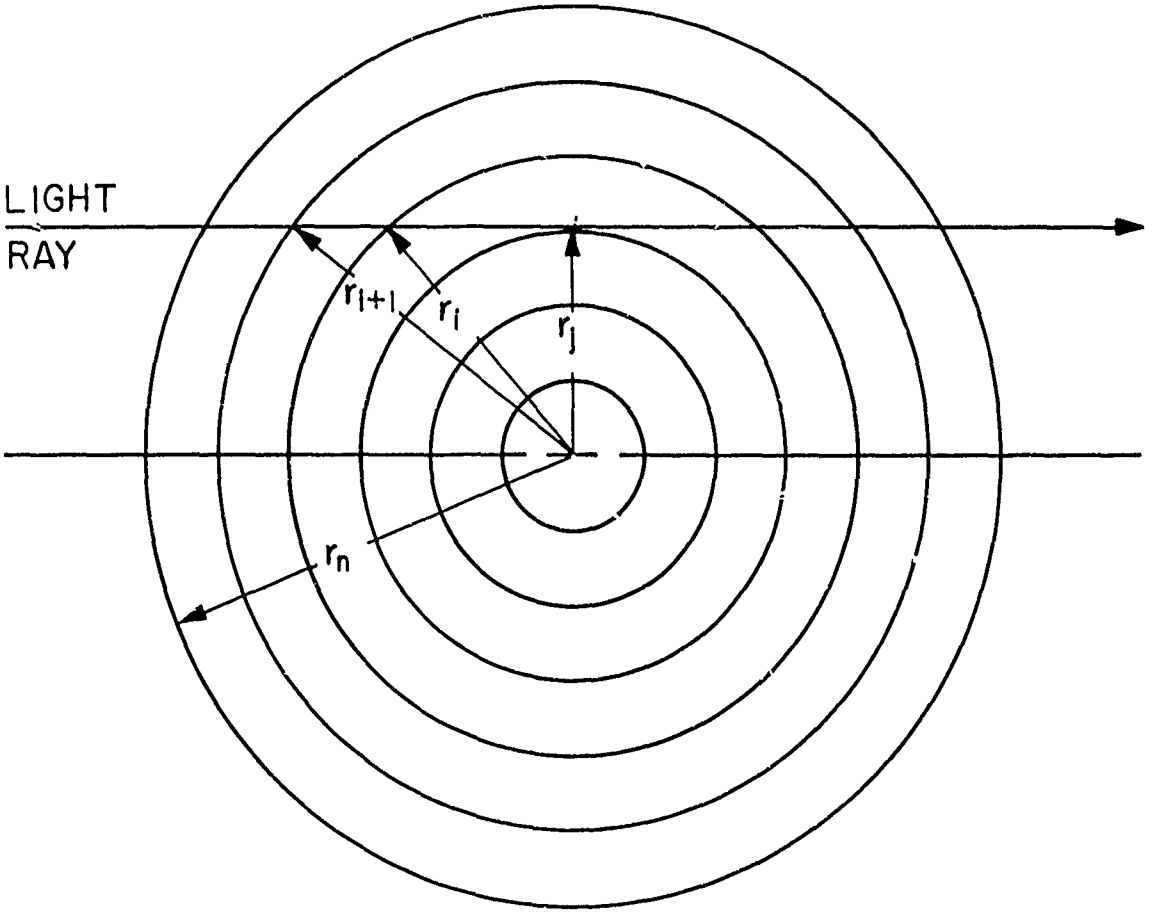

Fig. 3 — A cross section of a reduced density channel showing the subdivision into concentric shells used to invert the data

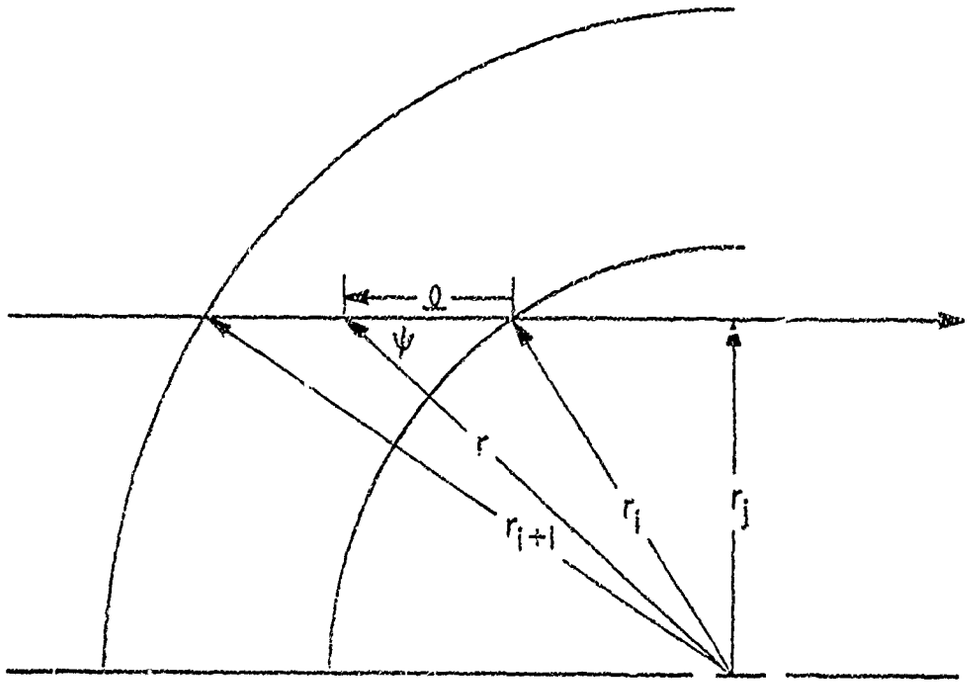

Fig. 4 — A diagram of one shell showing the relationships between the variables r, ψ, and l and the parameters r_j, r_i, and r_{j+1}.

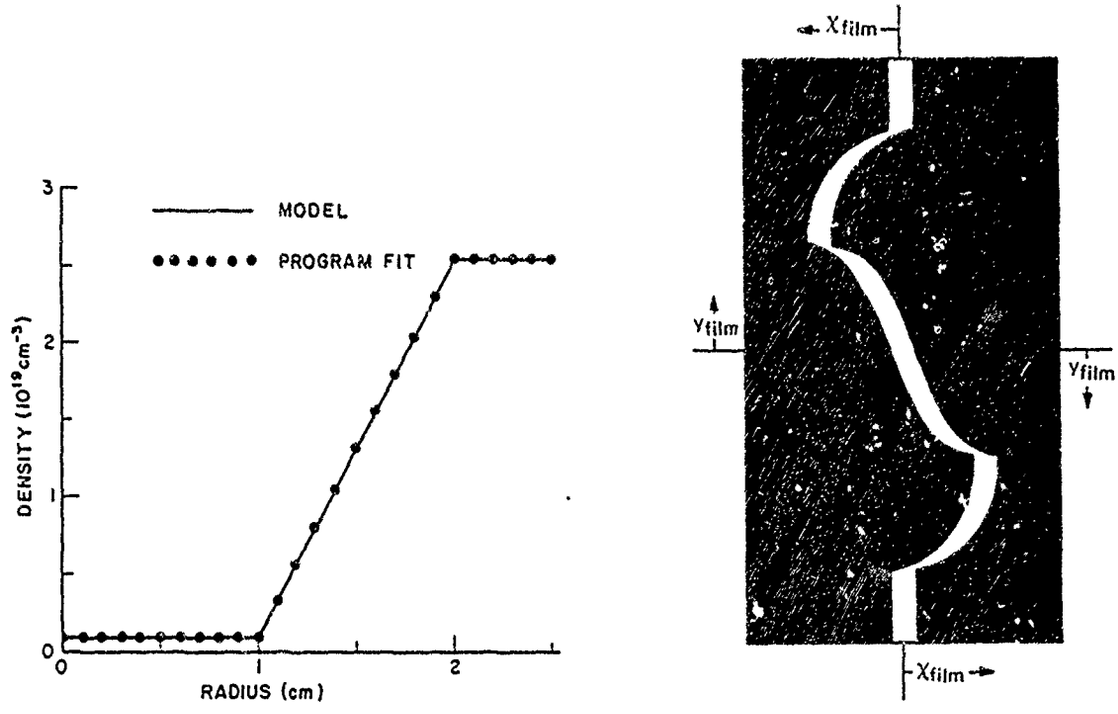

Fig. 5 — a) The analytic density profile used to test the inversion program and the fit achieved by the program. b) A hypothetical photograph constructed from the test data for the analytic model.

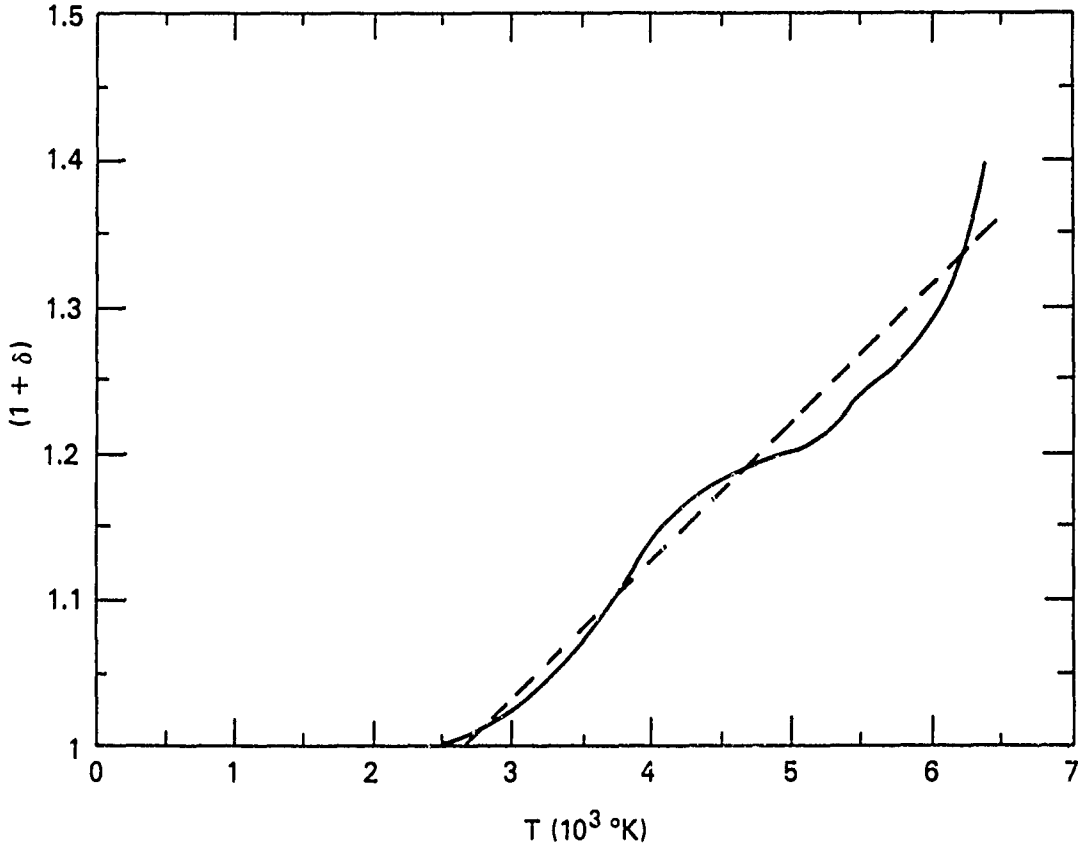

Fig 6 — A plot of (1+δ) as a function of temperature for atmospheric air where δ is the fractional dissociation. The plot is based on the tables of Burhorn and Wienecke[14]. The dotted line gives the approximation used by the program.

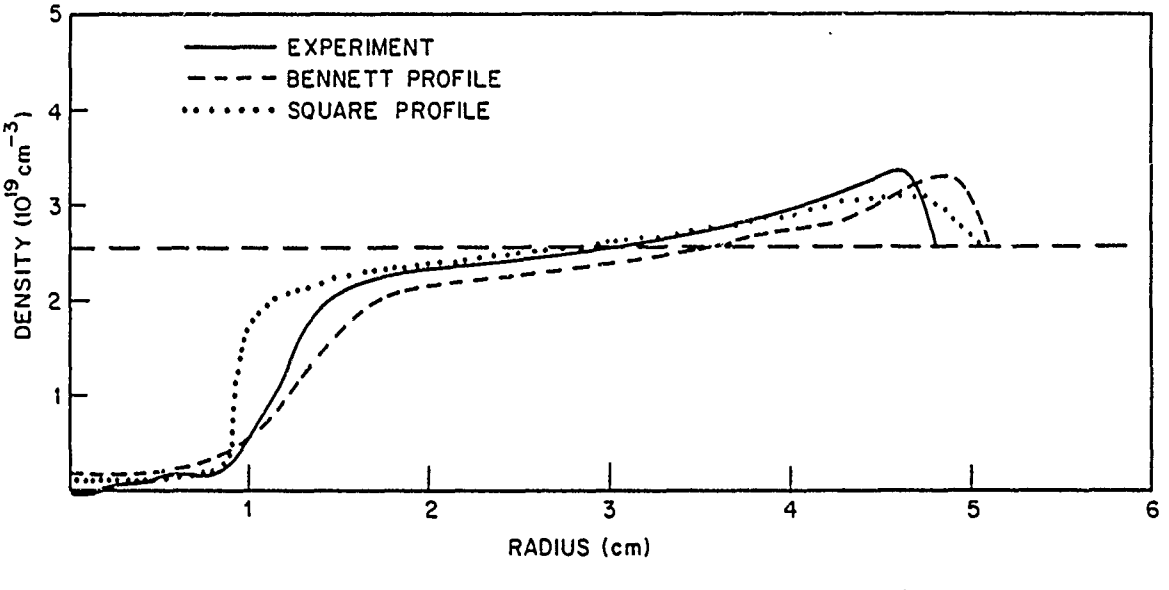

Fig 7 — The measured density profile for the channel in Fig. 2 compared to numerical simulations for two possible initial conditions. The simulations correspond to an instantaneous deposition of energy equal to the ohmic heating with either a square or Bennett radial profile. The characteristic radius in each case is the radius of the laser disturbance which guided the ohmic heating pulse.

DISTRIBUTION LIST

1. Commander
   Naval Sea Systems Command
   Department of the Navy
   Washington, D.C. 20363
   ATTN: NAVSEA 03H (Dr. C.F. Sharn)

2. Central Intelligence Agency
   P.O. Box 1925
   Washington, D.C. 20013
   ATTN: Dr. C. Miller/OSI

3. Air Force Weapons Laboratory
   Kirtland Air Force Base
   Albuquerque, New Mexico 87117
   ATTN: Lt. Col. J.H. Havey

4. U.S. Army Ballistics Research Laboratory
   Aberdeen Proving Ground, Maryland 21005
   ATTN: Dr. D. Eccleshall (DRXBR-BM)

5. Ballistic Missile Defense Advanced Technology Center
   P.O. Box 1500
   Huntsville, Alabama 35807
   ATTN: Dr. L. Harvard (BMDSATC-1)

6. B-K Dynamics Inc.
   15825 Shady Grove Road
   Rockvile, Maryland 20850
   ATTN: Mr. I. Kuhn

7. Intelcom Rad Tech
   P.O. Box 81087
   San Diego, California 92183
   ATTN: Mr. W. Selph

8. Lawrence Livermore Laboratory
   University of California
   Livermore, California 94550
   ATTN: Dr. R.J. Briggs
   Dr. T. Fessenden
   Dr. E.P. Lee

9. Mission Research Corporation
   735 State Street
   Santa Barbara, California 93102
   ATTN: Dr. C. Longmire
   Dr. N. Carron

10. National Bureau of Standards
    Gaithersburg, Maryland 20760
    ATTN: Dr. Mark Wilson

11. Science Applications, Inc.
1200 Prospect Street
LaJolla, California 92037
ATTN: Dr. M.P. Fricke
Dr. W.A. Woolson

12. Science Applications, Inc.
Security Office
5 Palo Alto Square, Suite 200
Palo Alto, California 94304
ATTN: Dr. R.R. Johnston
Dr. Leon Feinstein

13. Science Applications, Inc.
1651 Old Meadow Road
McLean, Virginia 22101
ATTN: Mr. W. Chadsey

14. Science Applications, Inc.
8201 Capwell Drive
Oakland, California 94621
ATTN: Dr. J.E. Reaugh

15. Naval Surface Weapons Center
White Oak Laboratory
Silver Spring, Maryland 20910
ATTN: Mr. R.J. Biegalski
Dr. R. Cawley
Dr. J.W. Forbes
Dr. D.L. Love
Dr. C.M. Huddleston
Mr. W.M. Hinckley
Dr. G.E. Hudson
Mr. G.J. Peters
Mr. N.E. Scofield
Dr. E.C. Whitman
Dr. M.H. Cha
Dr. H.S. Uhm
Dr. R.B. Fiorito

16. C.S. Draper Laboratories
Cambridge, Massachusetts 02139
ATTN: Dr. E. Olsson
Dr. L. Matson

17. M.I.T. Lincoln Laboratories
P.O. Box 73
Lexington, Massachusetts 02173
ATTN: Dr. J. Salah

18. Physical Dynamics, Inc.
P.O. Box 1883
LaJolla, California 92038
ATTN: Dr. K. Brueckner

19. Office of Naval Research
Department of the Navy
Arlington, Virginia 22217
ATTN: Dr. W.J. Condell (Code 421)

20. Avco Everett Research Laboratory
2385 Revere Beach Pkwy.
Everett, Massachusetts 02149
ATTN: Dr. R. Patrick
Dr. Dennis Reilly

21. Defense Technical Information Center
Cameron Station
5010 Duke Street
Alexandria, VA 22314 (12 copies)

22. Naval Research Laboratory
Washington, D.C. 20375
ATTN: M. Lampe — Code 4792
M. Friedman — Code 4700.1
J.R. Greig — Code 4763 (50 copies)
I.M. Vitkovitsky — Code 4770
T. Coffey — Code 4000
Superintendent, Plasma Physics Div. — Code 4700 (25 copies)
Library — Code 2628 (20 copies)
A. Ali — Code 4700.1T
D. Book — Code 4040
J. Boris — Code 4040
S. Kainer — Code 4790
A. Robson — Code 4760
M. Picone — Code 4040
D. Spicer — Code 4169
M. Raleigh — Code 4763
R. Pechacek — Code 4763
J.D. Sethian — Code 4762
K.A. Gerber — Code 4762
D.N. Spector — Code 4762

23. Defense Advanced Research Projects Agency
1400 Wilson Blvd.
Arlington, Virginia 22209
ATTN: Dr. J. Mangano
Dr. J. Bayless

24. JAYCOR
205 S. Whiting St.
Alexandria, Virginia 22304
ATTN: Drs. D. Tidman
R. Hubbard
J. Gillory

25. JAYCOR
Naval Research Laboratory
Washington, D.C. 20375
ATTN: Dr. R. Fernsler — 4770
Dr. G. Joyce — Code 4790
Dr. S. Goldstein — Code 4770

26. SAI
Naval Research Laboratory
Washington, D.C. 20375
ATTN: A. Drobot — Code 4790
W. Sharp — Code 4790

27. Physics International, Inc.
2700 Merced Street
San Leandro, CA
ATTN: Dr. J. Maenchen
Dr. E. Goldman

28. Mission Research Corp.
1400 San Mateo, S.E.
Albuquerque, NM 87108
ATTN: Dr. Brendan Godfrey

29. Princeton University
Plasma Physics Laboratory
Princeton, NJ 08540
ATTN: Dr. F. Perkins, Jr.

30. McDonnell Douglas Research Laboratories
Dept. 223, Bldg. 33, Level 45
Box 516
St. Louis, MO 63166
ATTN: Dr. Michael Greenspan

31. Cornell University
Ithaca, NY 14853
ATTN: Prof. David Hammer

32. Sandia Laboratories
Albuquerque, NM 87185
ATTN: Dr. Bruce Miller
Dr. Barbara Epstein
Dr. John Olsen
Dr. Don Cook

33. University of California
Physics Department
Irvine, CA 92717
ATTN: Dr. Gregory Benford

34. Naval Air Systems Command
Washington, D.C. 20361
ATTN: Dr. R.J. Wasneski, Code AIR-350F

35. Beers Associates, Inc.
P.O. Box 2549
Reston, VA 22090
ATTN: Dr. Douglas Strickland

36. U.S. Department of Energy
Washington, D.C. 20545
Office of Fusion Energy, ATTN: Dr. W. F. Dove
Office of Inertial Fusion, ATTN: Dr. T. Godlove

37. AFOSR/NP
Bolling Air Force Base
Washington, D.C. 20331
ATTN: Capt. R.L. Gullickson